NeuroImage: Clinical 3 (2013) 212–217

Contents lists available at ScienceDirect

NeuroImage: Clinical

journal homepage: www.elsevier.com/locate/ynicl

[^{123}I]-IBVM SPECT imaging of cholinergic systems in multiple system atrophy: A specific alteration of the ponto-thalamic cholinergic pathways (Ch5–Ch6)☆

Joachim Mazere [a,b,c,*,1], Wassilios. G. Meissner [d,e,f,1], Igor Sibon [a,b], Frédéric Lamare [a,b,c], François Tison [d,e,f], Michèle Allard [a,b,c,g], Willy Mayo [a,b]

[a] Univ. Bordeaux, INCIA, UMR 5287, F-33400 Talence, France
[b] CNRS, INCIA, UMR 5287, F-33400 Talence, France
[c] CHU de Bordeaux, Service de Médecine Nucléaire, Bordeaux, France
[d] Univ. de Bordeaux, Institut des Maladies Neurodégénératives, UMR 5293, F-33000 Bordeaux, France
[e] CNRS, Institut des Maladies Neurodégénératives, UMR 5293, F-33000 Bordeaux, France
[f] CHU de Bordeaux, Service de Neurologie et Centre de Référence Atrophie Multisystématisée, Pessac, France
[g] EPHE, France

ARTICLE INFO

Article history:
Received 8 July 2013
Received in revised form 30 July 2013
Accepted 31 July 2013
Available online xxxx

Keywords:
Single Photon Emission Computed Tomography
[^{123}I]-iodobenzovesamicol
Vesicular acetylcholine transporter
Multiple System Atrophy
Pharmacokinetic modeling

ABSTRACT

We evaluated *in vivo* the integrity of brain cholinergic pathways in Multiple System Atrophy (MSA) and the relationship between cholinergic dysfunction and motor disturbances, by measuring the vesicular acetylcholine transporter (VAChT) expression using Single Photon Emission Computed Tomography (SPECT) and [^{123}I]-iodobenzovesamicol ([^{123}I]-IBVM).

Methods: Nine patients with probable MSA and 12 healthy volunteers underwent a dynamic [^{123}I]-IBVM SPECT–CT scan and a magnetic resonance imaging (MRI) scan. All patients were examined with the Unified MSA Rating Scale (UMSARS; subscale I = activities of daily living (ADL), II = motor and IV = disability). CT and MRI images were used to register the dynamic SPECT image to the Montreal Neurological Institute brain template, which includes the regions of interest (ROI) of striatum and Ch1 (medial septum nucleus-hippocampus), Ch4 (nucleus basalis of Meynert-cortex) and Ch5–Ch6 (pedunculopontine and laterodorsal tegmental nuclei-thalamus) cholinergic pathways. For each ROI, pharmacokinetic modeling of regional time activity curves led to the calculation of [^{123}I]-IBVM to VAChT binding potential (BP_{ND}) value, proportional to VAChT expression.

Results: When compared to controls, BP_{ND} values for MSA in Ch5–Ch6 were significantly decreased in both the pedunculopontine–laterodorsal nuclei and the thalamus ($p = 0.004$ and $p = 0.006$, respectively). Additionally, thalamus BP_{ND} values were correlated with UMSARS ADL ($p = 0.006$), motor ($p = 0.002$) and disability ($p = 0.02$) sub-scores. UMSARS motor subscale items 13 (postural instability) and 14 (gait) were also correlated with thalamus BP_{ND} values ($p = 0.04$).

Conclusion: Ch5–Ch6 are the most affected cholinergic pathways in MSA at both cell bodies and thalamic cholinergic terminals. These results underscore the relevant role of [^{123}I]-IBVM SPECT for improving our understanding of the pathophysiology in MSA.

1. Introduction

Multiple System Atrophy (MSA) is an adult-onset progressive neurodegenerative disease characterized by a variable combination of parkinsonism, cerebellar ataxia, autonomic failure and pyramidal signs (Stefanova et al., 2009; Watanabe et al., 2002).

As in Parkinson's disease (PD), the loss of nigro-striatal dopamine neurons causes the onset of parkinsonian motor signs in MSA. However, in contrast to PD, MSA patients show a poor response to dopaminergic drugs, suggesting additional involvement of non-dopaminergic systems. In this view, *post-mortem* studies have revealed a loss of mesopontine cholinergic neurons (Schmeichel et al., 2008). Moreover, *in vivo* imaging

* Corresponding author at: Service de Médecine Nucléaire, Hôpital du Haut-Lévêque, Avenue de Magellan, F-33604 Pessac Cedex, France. Tel.: +33 5 57 65 64 08; fax: +33 5 57 65 68 39.
E-mail address: joachim.mazere@chu-bordeaux.fr (J. Mazere).

[1] The two authors contributed equally to this work.

2213-1582/$ – see front matter © 2013 The Authors. Published by Elsevier Inc. All rights reserved.
http://dx.doi.org/10.1016/j.nicl.2013.07.012

Table 1
Patient demographics and UMSARS scores.

Patient no.	Type	Age (years)	Gender	Disease duration (years)	UMSARS ADL	UMSARS motor	UMSARS disability
1	MSA-P	70	F	3	21	21	2
2	MSA-P	65	M	10	25	40	3
3	MSA-P	72	M	4	17	20	1
4	MSA-C	59	M	6	18	20	2
5	MSA-C	56	M	5	26	23	1
6	MSA-C	62	M	7	16	25	2
7	MSA-C	59	M	5	40	45	4
8	MSA-C	61	M	2	21	22	2
9	MSA-C	63	M	5	31	29	3

studies have shown a decrease of acetylcholinesterase (AChE) activity in both cortical and subcortical structures (Gilman et al., 2010) and a decrease of the vesicular acetylcholine transporter (VAChT) in the thalamus (Gilman et al., 2003). Subcortical AChE activity is further correlated with gait disturbances (Gilman et al., 2010) and VAChT expression in the thalamus has an inverse correlation with the severity of obstructive sleep apnea (Gilman et al., 2003). The thalamus is the main projection area of cholinergic neurons originating from the pedunculopontine (PPT) and laterodorsal tegmental nuclei. The results of previous studies therefore suggest an important role of dysfunction of the Ch5–Ch6 (ponto-thalamic) cholinergic pathways in the pathophysiology of MSA. However, although the PPT–LDT are thought to play a pivotal role in the genesis of motor disorders and the control of the sleep–wake cycle and attention (Jenkinson et al., 2009), the integrity of cholinergic neurons in these nuclei has never been studied *in vivo* in MSA. This is partly due to technical problems, namely the small size of the PPT and LDT. In order to overpass this problem, we recently proposed a new method of *in vivo* quantification of VAChT expression in Single Photon Emission Computed Tomography (SPECT) imaging, using anatomical image to brain atlas non-rigid registration (Lamare et al., 2013).

We extend here the findings of previous *in vivo* studies in MSA (Gilman et al., 2010, 2003) by exploring the integrity of the Ch5–Ch6 cholinergic pathways by SPECT with [^{123}I]-iodobenzovesamicol ([^{123}I]-IBVM), a selective radioligand of the VAChT (Kuhl et al., 1994; Mazere et al., 2012). Cell bodies in the PPT and terminals in the thalamus were assessed, as well as the relationship between cholinergic denervation and motor disturbances. We also explored the Ch4 (nucleus basalis of Meynert-cortical (Wevers, 2011)) and Ch1 (septo-hippocampal (Wevers, 2011)) cholinergic pathways at both levels, cell bodies (basal forebrain cholinergic nuclei) and terminals, *i.e.* cortical regions for the Ch4 and hippocampus for the Ch1.

2. Materials and methods

2.1. Subjects

Twenty one subjects were included after written informed consent: 9 patients with "probable" MSA (8 men, 1 woman) were recruited at the French Reference Centre for MSA (University Hospital of Bordeaux) and 12 healthy volunteers (3 men, 9 women) without neurological and neuropsychiatric disorders. The diagnosis of MSA was made according to consensus criteria (Gilman et al., 1999). Six patients had probable MSA-C and three had probable MSA-P at the moment of the imaging protocol. All patients were evaluated with the Unified MSA Rating Scale (UMSARS; subscale I = activities of daily living (ADL), II = motor and IV = disability). The diagnosis of MSA was confirmed *post-mortem* in three patients who came to necropsy after the end of the study.

2.2. Standard protocol approvals, registrations and patient consent

The study was initiated after protocol approval by the institutional Human Ethics Committee and radioactive drug approval by the National Health Product Safety Agency. Before providing written consent, all participants were presented with the basic design of the study and were informed that they could withdraw from the investigation at anytime.

2.3. Radiochemistry

[^{123}I]-IBVM was prepared and controlled as previously described (Mazere et al., 2008). Briefly, after radio-iodination, [^{123}I]-IBVM was purified by High Pressure Liquid Chromatography and Sep-PackC18 classic cartridge (Waters; Milford, MA) and filtered, leading to 10 ml of sterile solution of [^{123}I]-IBVM. Prior to injection, the solution was assessed to

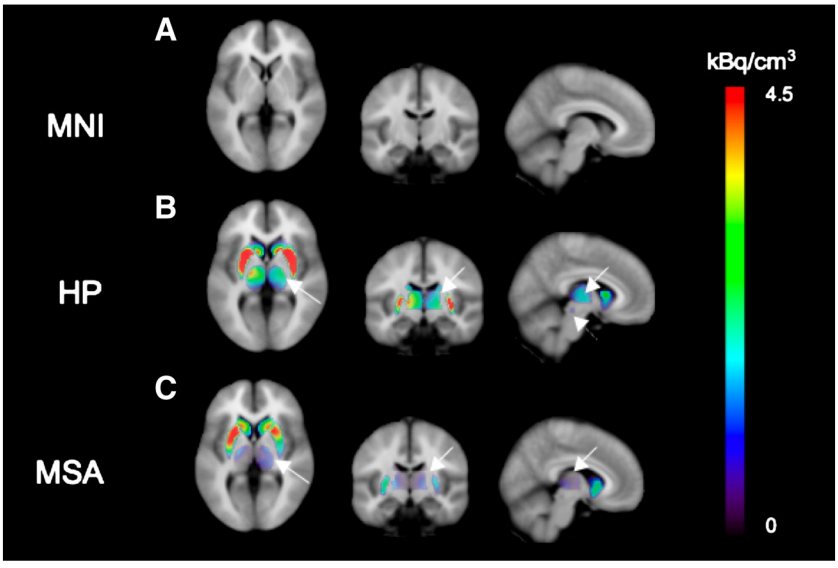

Fig. 1. Representative SPECT images of a healthy participant and patient with MSA. MNI MR imaging template (row A) and representative example of SPECT images acquired at 7 h after injection for healthy participant (HP, row B) and patient with MSA (row C). For each row, three images, from left to right, are transverse, coronal and sagittal views. Specific binding in striatum, thalamus and PPT–LDT regions has been extracted from SPECT images by calculating difference (region of interest activity concentration (*i.e.* total binding) − reference region activity concentration (*i.e.* non specific binding)) and is presented overlaid (B, C) with the MNI T1 MR imaging template. Solid white arrows label the thalamus and dotted white arrow labels the pedunculopontine and laterodorsal tegmental nuclei. For patient with MSA, specific binding is visually lower in thalamus than for healthy participant.

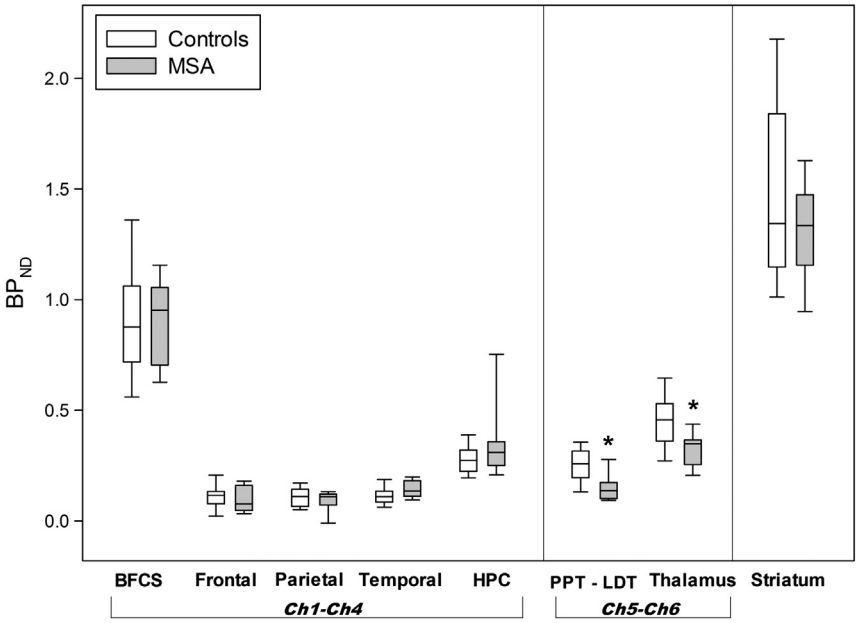

Fig. 2. Box plots showing BP_{ND} values calculated in Ch1–Ch4, Ch5–Ch6 and striatal cholinergic interneurons of healthy subjects and MSA patients. The line within the box marks the median, boundaries above and below indicates the 75th and 25th percentile respectively. Whiskers above and below the box indicates the 90th and 10th percentiles. Abbreviations: BFCS: basal forebrain cholinergic system; HPC: hippocampus; PPT–LDT: pedunculopontine and laterodorsal tegmental nuclei. *$p \leq 0.006$.

be pyrogen-free using the Endosafe-PTS portable test system (Charles River Laboratories, Wilmington, MA).

2.4. Scanning protocol

2.4.1. Anatomic MR imaging

For anatomical localization and partial volume effect (PVE) correction of the SPECT data, subjects underwent a three-dimensional T1 MR imaging sequence (repetition time (TR)/echo time (TE), 7.1/3.5 ms; flip angle, 8°; field of view, 256 × 256 mm to cover the whole brain yielding 228 slices and slice thickness of 1 mm; voxel size, 1 mm^3) using a 1.5-T MR imaging system (Philips, Best, The Netherlands).

2.4.2. SPECT–CT imaging

SPECT imaging was performed on a SPECT/CT SYMBIA T2 camera (Siemens; Erlangen, Germany) equipped with low energy thin section collimators. The participants were given 400 mg of potassium perchlorate orally 30 min before and 24 h after imaging. After a mean intravenous injection of 267.02 ± 33.91 MBq of [^{123}I]-IBVM, the dynamic SPECT images were acquired over 7 h at five different times: five frames of 6 min at injection time and two 15-min frames at 1 h, 2.5 h, 4.5 h and 7 h after injection (64 projections with a matrix of 64 × 64 over 360°).

Table 2
Correlation between imaging (BP_{ND} values) and clinical data.

Imaging data	Thalamus BP_{ND}		PPT–LDT BP_{ND}	
	Correlation coefficent	*p*	Correlation coefficent	*p*
Age	0.041	0.92	0.510	0.16
Disease duration	−0.300	0.43	0.493	0.18
UMSARS ADL	−0.823	**0.006**	−0.0319	0.94
UMSARS motor				
Total	−0.881	**0.002**	0.243	0.53
Item 13 (instability)	−0.684	**0.04**	0.522	0.15
Item 14 (gait)	−0.684	**0.04**	0.213	0.58
UMSARS disability	−0.762	**0.02**	0.0665	0.87

PPT–LDT = Pedunculopontine and laterodorsal tegmental nuclei; Bold = $p < 0.05$.

Between each of the five acquisitions, the participants were allowed to rest outside of the gantry.

SPECT images were reconstructed on a 64 × 64 matrix by using a flash three-dimensional iterative reconstruction (four iterations, eight subsets) and a voxel size of 6.8 × 6.8 × 6.8 mm^3. With low energy high resolution collimators, the reconstructed spatial resolution of the images was ≤5.8 mm (center), ≤5.0 mm (radial) and ≤4.1 mm (tangential). Attenuation correction was performed using the CT image.

All reconstructed images were post-processed, including decay correction, normalization for frame duration and frame merging. All the frames were rigidly registered together and with the CT image, to ensure the patient's brain was in the exact same position in all the images during the creation of the dynamic SPECT dataset.

2.5. SPECT data registration to the Montreal Neurological Institute template

The anatomical images, CT and MRI were used to register the dynamic [^{123}I]-IBVM SPECT image to the Montreal Neurological Institute (MNI) template and the associated set of brain regions of interests (ROIs). The acquisition and processing protocol involved three main steps: 1) The participants' CT and MR images were coregistered by using a rigid registration. Because these two images corresponded to the same participant, a rigid model (three translations and three rotations) was sufficient. The rigid transformation parameters were subsequently applied to the dynamic SPECT data to ensure the coregistration with the patients' MR images. 2) The participants' MR images were segmented to extract the skull and cerebrospinal fluid and to only preserve the voxels corresponding to the white and gray tissues of the brain. This process was necessary to obtain an MR image with similar anatomic information as the MNI template from which images of the skull and the cerebrospinal fluid were removed. 3) Finally, the MR craniumless scan was spatially coregistered with the MNI T1-weighted brain template by using an elastic registration algorithm (FSL software, Oxford, United Kingdom). The transformations resulting from 1) and 3) were subsequently applied to the four-dimensional SPECT dataset that had previously been aligned with the participants' MR images, providing a four-dimensional SPECT image registered to the MNI template.

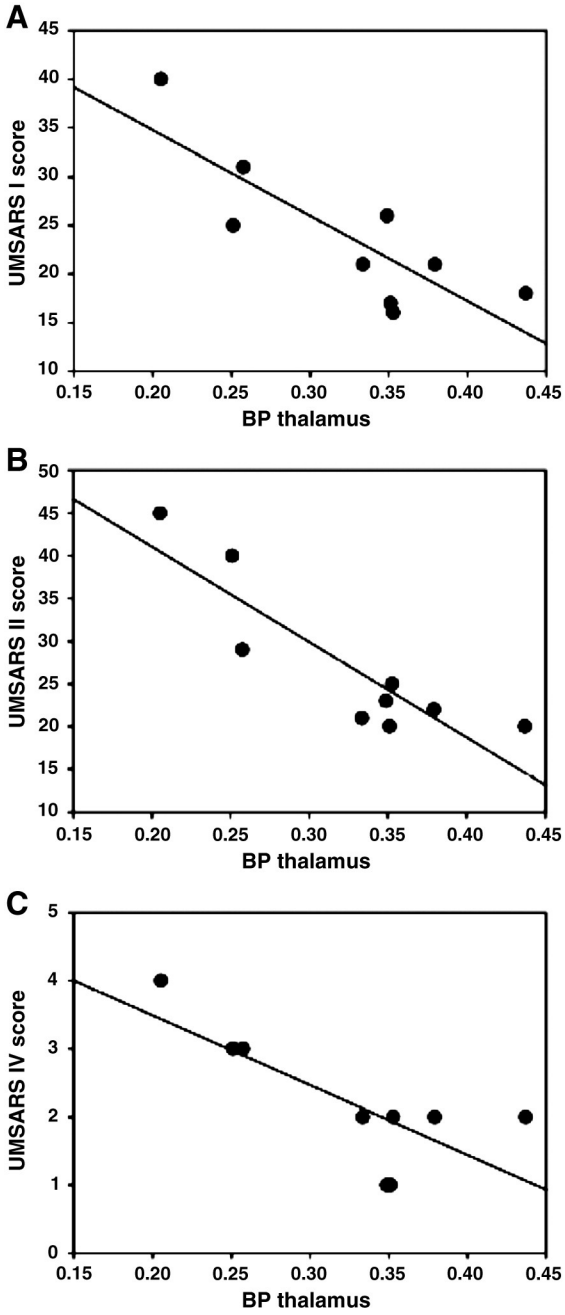

Fig. 3. Scatter plot with regression line of UMSARS sub-scores and thalamic binding potentials. UMSARS I (A), UMSARS II (B) and UMSARS IV (C) sub-scores strongly correlated with thalamic binding potentials.

2.6. Pharmacokinetic modeling

2.6.1. Partial volume effect correction of the normalized dynamic SPECT dataset

For partial volume effect correction of the four-dimensional SPECT image registered to the MNI template, extracerebral tissue (*i.e.* cerebrospinal fluid plus cranium) was eliminated on MR images of each participant by using an SPM5 (Wellcome Department of Imaging Neuroscience, London, England) automatic two-segment (brain tissue and cerebrospinal fluid) MR segmentation method (Giovacchini et al., 2004). The resulting mask, shown to be sufficient in studies of neurodegenerative diseases (Meltzer et al., 1999), was applied voxel-by-voxel to the four-dimensional SPECT image, resulting in unchanged voxels in the MR-derived white and gray matter and voxels set to 0 in the cerebrospinal fluid and cranium regions (Giovacchini et al., 2004).

Finally, for each participant, an MNI-registered and partial volume effect-corrected dynamic SPECT data was obtained and transferred to PMOD software (version 3.1, PMOD Technologies, Zurich, Switzerland; http://www.pmod.com) for derivation of regional time–activity curves.

2.6.2. Time–activity curve calculation

A template in the MNI space was created on the basis of the anatomic automatic labeling brain segmentation (Tzourio-Mazoyer et al., 2002). The template was built by merging some of the anatomic automatic labeling brain segmentation regions to define ROIs of striatum for pharmacokinetic modeling, and the three main anatomic cholinergic pathways: Ch1, including medial septum and hippocampus; Ch4, including nucleus basalis of Meynert (NbM); frontal, parietal and temporal cortices; and Ch5-Ch6, including pedunculopontine (PPT) and laterodorsal (LDT) nuclei and thalamus. We created volumes of interest surrounding each nucleus in the MNI space. The NbM, PPT–LDT and medial septum volumes were respectively 2×15^3, 2×9^3 and 2×9^3 voxels, respectively. Finally, the NbM and medial septum were merged together, providing the region of "the basal forebrain cholinergic nuclei".

The PMOD software was used to apply this template to each frame of the registered and partial volume effect-corrected dynamic SPECT data to obtain average-decay corrected regional activities, which were plotted against time to get regional time–activity curves.

2.6.3. Pharmacokinetic model

In a previous study (Barret et al., 2008), multilinear analysis by using multilinear reference tissue model 2 was shown to give the best correlation between results by using the occipital cortex as a reference region and results from invasive blood-sampling analysis (Kuhl et al., 1994). Therefore, the multilinear reference tissue model 2 method was considered to be the method of choice for non-invasive quantification of [^{123}I]-IBVM data. A two-step approach used with multilinear reference tissue model 2, combining calculation of the reference region-to-plasma k'_2 and multilinear regression analysis (Barret et al., 2008), for each ROI, led to the calculation of the non-displaceable binding potential (BP_{ND}) value, a parameter whose value is proportional to the density of receptor sites, in this case, VAChT binding sites. The occipital cortex was chosen as a reference region because, in this area, post-mortem choline acetyltransferase levels (Araujo et al., 1988) – an enzyme distributed in the same way as VAChT in the human brain (Erickson et al., 1994; Kuhl et al., 1996) – and *in vivo* specific binding of [^{123}I]IBVM (Kuhl et al., 1994; Mazere et al., 2012) were both shown to be very low.

In our study, we applied the same method and calculated [^{123}I]-IBVM to VAChT BP_{ND} values for each participant and each ROI.

2.7. Statistical analysis

Mann–Whitney *U* tests were used to test differences in BP_{ND} values in each ROI between control participants and patients with MSA. The results of the present study included corrections for multiple comparisons: with eight regions examined, a conservative multiple comparisons by using Bonferroni adjustment required a significance level of $p < 0.006$.

Correlations between BP_{ND} values in each ROI and age, disease duration and clinical data (UMSARS I, II and IV subscores) were assessed by using Pearson correlations. Statistical analyses were performed using STATISTICA software version 9 (Statsoft; Tulsa, OK, USA: http://www.statsoft.com).

3. Results

3.1. Subject characteristics

MSA patients (63.0 ± 5.2 years) were significantly younger than healthy subjects (69.8 ± 4.7 years; $p < 0.01$). The male–female ratio was higher in patients with MSA than in controls. Mean disease duration was 5.2 ± 2.3 years (Table 1). Mean UMSARS ADL scores were

23.9 ± 7.7, mean UMSARS motor scores were 27.2 ± 9.2 and mean UMSARS disability scores were 2.2 ± 1.0.

3.2. Cholinergic pathways integrity assessment

In Ch5–Ch6, BP_{ND} values for MSA were significantly decreased in both the PPT–LDT and the thalamus ($p = 0.004$ and $p = 0.006$, respectively) comparatively to control participants (Figs. 1 and 2). On the contrary, in Ch4 and Ch1, no significant differences in BP_{ND} values were observed between patients with MSA and control participants whatever the level, cell bodies and terminals (Fig. 2).

No correlation was found between BP_{ND} values and age irrespective of the ROI and the group, suggesting that age differences between groups did not affect BP_{ND} values.

3.3. Correlation between BP_{ND} and clinical markers

Thalamus BP_{ND} values were correlated with UMSARS ADL ($p = 0.006$), motor ($p = 0.002$) and disability ($p = 0.02$) sub-scores, while no correlation was found with disease duration (Table 2, see also Fig. 3). UMSARS motor subscale items 13 (postural instability) and 14 (gait) were also correlated with thalamus BP_{ND} values ($p = 0.04$). No correlation was found between PPT–LDT BP_{ND} values, disease duration and clinical data.

4. Discussion

The main result of the present study is the significant alteration of the Ch5–Ch6 pathways in MSA with a relative preservation of Ch1 and Ch4 pathways. We further found a significant correlation between BP_{ND} values in the thalamus and UMSARS ADL, motor and disability scores suggesting progressive cholinergic denervation with increasing disease burden.

The observation that [^{123}I]-IBVM binding is only reduced in the PPT–LDT nuclei and their connecting projection area, the thalamus, supports the hypothesis of a specific ponto-thalamic cholinergic degeneration in MSA. This result is consistent with a *post-mortem* analysis revealing a loss of PPT–LDT cholinergic neurons in MSA patients (Schmeichel et al., 2008) and anatomical data showing that PPT–LDT cholinergic neurons are mainly connected to the thalamus (Schmeichel et al., 2008). From a functional point of view, cholinergic PPT–LDT damage is consistent with clinical observations, as these cholinergic nuclei are implicated in the coordination of gait (Jenkinson et al., 2009), the latter being severely impaired in MSA. Although we did not find a significant correlation between BP_{ND} values in the PPT–LDT and UMSARS subscores, a strong argument for the involvement of the Ch5–Ch6 cholinergic network in motor features in MSA is provided by the significant correlation between thalamic BP_{ND} values and UMSARS motor scores including item scores for postural instability and gait. The absence of a correlation between PPT–LDT BP_{ND} values and clinical markers could result from the existence of different cholinergic sub-populations in these nuclei (Mesulam et al., 1989) and limited power of the study for such an analysis given the small sample size.

The absence of cortical cholinergic denervation in both Ch4 and Ch1 cholinergic pathways is in agreement with recent findings in MSA patients showing normal *in vivo* brain AChE activity (Hirano et al., 2008), however not reported in another study (Gilman et al., 2010).

Quantification of cholinergic neurons in small structures like the PPT–LDT is questionable when using a low resolution imaging technique such as SPECT. Nevertheless, several lines of evidence support its technical feasibility. First, quantification of the weak signal observed requires adapted image analysis methods. In this regard, modeling based BP_{ND} calculations have proven to be preferable methods. Therefore, given that our quantification relies on a fully automated method, the SPECT resolution can be improved if quantitative analysis relies on an exact identification of the different brain regions. This is why reliability of SPECT to MRI registration is crucial. Thus, we chose an elastic based registration algorithm, which is able to account for local deformation, particularly if the subject's MRI is affected by cerebral atrophy (Lamare et al., 2013). Secondly, the low SPECT resolution could be a limitation when studying adjacent and very small cholinergic structures. However, this problem should not be relevant for small cholinergic structures not closely surrounded by other adjacent cholinergic structures, such as the PPT, which is, with the LDT, the only cholinergic structure located in the pons area (Jenkinson et al., 2009).

The significant age and gender differences between patient and control group merit consideration as a study limitation, although there was no direct correlation of BP_{ND} values and age.

5. Conclusion

Our results strongly support the hypothesis that Ch5–Ch6 are the most affected cholinergic pathways in MSA, with significant neuronal loss affecting both PPT–LDT cell bodies and thalamic cholinergic terminals. These results underscore the relevant role of [^{123}I]-IBVM SPECT for studying the integrity of cholinergic pathways and for improving our understanding of the pathophysiology in MSA. Given the parallel alteration of the dopaminergic systems in this pathology, it would be interesting to explore subsequently *in vivo* in MSA patients both cholinergic and dopaminergic neurotransmission, for a better understanding of the relationship between motor disturbances and neurotransmitter changes.

Acknowledgments

The authors thank Eisai Pharmaceuticals Company, Tokyo, Japan for the financial support to M.A. They also thank Denis Guilloteau, Caroline Buisson for protocol management and Thierry Blandin for technical assistance.

References

Araujo, D.M., Lapchak, P.A., Robitaille, Y., Gauthier, S., Quirion, R., 1988. Differential alteration of various cholinergic markers in cortical and subcortical regions of human brain in Alzheimer's disease. Journal of Neurochemistry 50, 1914–1923.

Barret, O., Mazere, J., Seibyl, J., Allard, M., 2008. Comparison of noninvasive quantification methods of in vivo vesicular acetylcholine transporter using [^{123}I]-IBVM SPECT imaging. Journal of Cerebral Blood Flow and Metabolism 28, 1624–1634.

Erickson, J.D., Varoqui, H., Schafer, M.K., Modi, W., Diebler, M.F., Weihe, E., Rand, J., Eiden, L.E., Bonner, T.I., Usdin, T.B., 1994. Functional identification of a vesicular acetylcholine transporter and its expression from a "cholinergic" gene locus. Journal of Biological Chemistry 269, 21929–21932.

Gilman, S., Low, P.A., Quinn, N., Albanese, A., Ben-Shlomo, Y., Fowler, C.J., Kaufmann, H., Klockgether, T., Lang, A.E., Lantos, P.L., Litvan, I., Mathias, C.J., Oliver, E., Robertson, D., Schatz, I., Wenning, G.K., 1999. Consensus statement on the diagnosis of multiple system atrophy. Journal of Neurological Sciences 163, 94–98.

Gilman, S., Chervin, R.D., Koeppe, R.A., Consens, F.B., Little, R., An, H., Junck, L., Heumann, M., 2003. Obstructive sleep apnea is related to a thalamic cholinergic deficit in MSA. Neurology 61, 35–39.

Gilman, S., Koeppe, R.A., Nan, B., Wang, C.N., Wang, X., Junck, L., Chervin, R.D., Consens, F., Bhaumik, A., 2010. Cerebral cortical and subcortical cholinergic deficits in parkinsonian syndromes. Neurology 74, 1416–1423.

Giovacchini, G., Lerner, A., Toczek, M.T., Fraser, C., Ma, K., DeMar, J.C., Herscovitch, P., Eckelman, W.C., Rapoport, S.I., Carson, R.E., 2004. Brain incorporation of 11C-arachidonic acid, blood volume, and blood flow in healthy aging: a study with partial-volume correction. Journal of Nuclear Medicine 45, 1471–1479.

Hirano, S., Shinotoh, H., Arai, K., Aotsuka, A., Yasuno, F., Tanaka, N., Ota, T., Sato, K., Fukushi, K., Tanada, S., Hattori, T., Irie, T., 2008. PET study of brain acetylcholinesterase in cerebellar degenerative disorders. Movement Disorders 23, 1154–1160.

Jenkinson, N., Nandi, D., Muthusamy, K., Ray, N.J., Gregory, R., Stein, J.F., Aziz, T.Z., 2009. Anatomy, physiology, and pathophysiology of the pedunculopontine nucleus. Movement Disorders 24, 319–328.

Kuhl, D.E., Koeppe, R.A., Fessler, J.A., Minoshima, S., Ackermann, R.J., Carey, J.E., Gildersleeve, D.L., Frey, K.A., Wieland, D.M., 1994. In vivo mapping of cholinergic neurons in the human brain using SPECT and IBVM. Journal of Nuclear Medicine 35, 405–410.

Kuhl, D.E., Minoshima, S., Fessler, J.A., Frey, K.A., Foster, N.L., Ficaro, E.P., Wieland, D.M., Koeppe, R.A., 1996. In vivo mapping of cholinergic terminals in normal aging, Alzheimer's disease, and Parkinson's disease. Annals of Neurology 40, 399–410.

Lamare, F., Mazere, J., Attila, M., Mayo, W., De Clermont-Gallerande, H., Meissner, W., Fernandez, P., Allard, M., 2013. Improvement of in vivo quantification of [^{123}I]-iodobenzovesamicol in single-photon emission computed tomography/computed tomography using anatomic image to brain atlas nonrigid registration. Molecular Imaging 12, 288–299.

Mazere, J., Prunier, C., Barret, O., Guyot, M., Hommet, C., Guilloteau, D., Dartigues, J.F., Auriacombe, S., Fabrigoule, C., Allard, M., 2008. In vivo SPECT imaging of vesicular acetylcholine transporter using [(123)I]-IBVM in early Alzheimer's disease. NeuroImage 40, 280–288.

Mazere, J., Meissner, W.G., Mayo, W., Sibon, I., Lamare, F., Guilloteau, D., Tison, F., Allard, M., 2012. Progressive supranuclear palsy: in vivo SPECT imaging of presynaptic vesicular acetylcholine transporter with [^{123}I]-iodobenzovesamicol. Radiology 265, 537–543.

Meltzer, C.C., Kinahan, P.E., Greer, P.J., Nichols, T.E., Comtat, C., Cantwell, M.N., Lin, M.P., Price, J.C., 1999. Comparative evaluation of MR-based partial-volume correction schemes for PET. Journal of Nuclear Medicine 40, 2053–2065.

Mesulam, M.M., Geula, C., Bothwell, M.A., Hersh, L.B., 1989. Human reticular formation: cholinergic neurons of the pedunculopontine and laterodorsal tegmental nuclei and some cytochemical comparisons to forebrain cholinergic neurons. The Journal of Comparative Neurology 283, 611–633.

Schmeichel, A.M., Buchhalter, L.C., Low, P.A., Parisi, J.E., Boeve, B.W., Sandroni, P., Benarroch, E.E., 2008. Mesopontine cholinergic neuron involvement in Lewy body dementia and multiple system atrophy. Neurology 70, 368–373.

Stefanova, N., Bucke, P., Duerr, S., Wenning, G.K., 2009. Multiple system atrophy: an update. Lancet Neurology 8, 1172–1178.

Tzourio-Mazoyer, N., Landeau, B., Papathanassiou, D., Crivello, F., Etard, O., Delcroix, N., Mazoyer, B., Joliot, M., 2002. Automated anatomical labeling of activations in SPM using a macroscopic anatomical parcellation of the MNI MRI single-subject brain. NeuroImage 15, 273–289.

Watanabe, H., Saito, Y., Terao, S., Ando, T., Kachi, T., Mukai, E., Aiba, I., Abe, Y., Tamakoshi, A., Doyu, M., Hirayama, M., Sobue, G., 2002. Progression and prognosis in multiple system atrophy: an analysis of 230 Japanese patients. Brain, vol. 125, pp. 1070–1083 (2002/04/19 ed).

Wevers, A., 2011. Localisation of pre- and postsynaptic cholinergic markers in the human brain. Behavioural Brain Research 221, 341–355.